

# Diode Laser Based Water Vapor Differential Absorption Lidar: an Advanced Wavelength Selection

Phong Pham Le Hoai and Makoto Abo

Graduate School of System Design

Tokyo Metropolitan University, Tokyo 191-0065, Japan

E-mail: phamlehoai@gmail.com, abo@tmu.ac.jp

**Abstract**—The random and systematic errors are evaluated in order to select the optimum wavelengths for operating diode laser based water vapor differential absorption lidar. The selection process is applied for both February and August period due to the H<sub>2</sub>O density distinction. As a result, the online-wavelengths of 823.616 nm for February and 823.689 nm for August, respectively, and the offline-wavelength of 823.763 nm are decided to be the optimum wavelengths for our lidar system over Japan region.

**Keywords:** diode laser, water vapor differential absorption lidar, wavelength selection, and relative error.

## I. INTRODUCTION

The water vapor profile is significant for studying atmospheric activities related to meteorology, hydrology, and climate. In particular, water vapor (H<sub>2</sub>O) is an influential greenhouse gas causing climate change which is recently a global emerged issue. The water vapor measurements have been improved in terms of precision and resolution using advanced lidar technology. A typical technique, Raman lidar, is able to observe multiple gas constituents simultaneously but require costly calibration components and massive laser transmitters. The diode laser based differential absorption lidar (DIAL) appears to overcome these disadvantages.

DIAL method utilizing a pair of lasers tuned on and off the peak of gas absorption line can avoid the calibration issue in case of Raman lidar. Furthermore, the DIAL based on diode laser is affordable, compact, and wide range wavelength tuning near infrared region. It has applied in ground-based and airborne lidar measurements of water vapor and aerosol for high spatial and temporal profiles.

The average gas concentration is basically obtained from the ratio of return online and offline signals as well as the knowledge of gas absorption coefficients at online and offline wavelengths. In order to enhance the precise results and eliminate errors, the DIAL designing needs to be dealt with random errors such as signal detection errors, and systematic errors such as temperature relative errors and wavelength tuning errors. Our work aims at selecting the optimum wavelengths for diode laser based DIAL system by evaluating the wavelength sensitive to these kinds of errors.

In Section 2, the methodology of differential absorption lidar is described. Then, the optimum

wavelengths are evaluated and discussed in Section 3. Finally, the conclusions are given in Section 4.

## II. METHODOLOGY

The DIAL for pair of return lidar signals at online and offline wavelengths,  $S_{on}$  and  $S_{off}$ , can be simply described in a form of the average gas concentration,  $n$ , between ranges  $R_1$  and  $R_2$ , as

$$n = \frac{1}{2\Delta\sigma(R_2 - R_1)} \ln \left[ \frac{S_{on}(R_1)S_{off}(R_2)}{S_{on}(R_2)S_{off}(R_1)} \right], \quad (1)$$

where  $\Delta\sigma$  is the differential absorption cross section between the online and offline wavelengths [1].

The lidar signal  $S$  from range  $R$  is determined by

$$S(R) = \frac{(E/h\nu)A\eta\beta Qc\Delta t}{2R^2} \exp\left[-2\int_0^R \alpha dR\right], \quad (2)$$

where  $E$  is the laser pulse energy,  $A$  is the effective area of the receiver,  $\eta$  is the quantum efficiency of the detector,  $\beta$  is the total atmospheric volume backscattering coefficient,  $Q$  is the total efficiency of the receiver for the signal accumulation time  $\Delta t$ , and  $\alpha$  is the atmospheric extinction coefficient [1].

The total atmospheric backscatter includes the molecular backscatter and aerosol backscatter conducted from the assumed three layer aerosol model with a phase function of 0.023 sr<sup>-1</sup> [2]. While the most dominant atmospheric extinction, H<sub>2</sub>O absorption, is described as following section.

### 2.1 H<sub>2</sub>O absorption cross section

The H<sub>2</sub>O absorption cross section estimation contains pressure and Doppler broadening half-width at half-maximum,  $\gamma_L$  and  $\gamma_D$ , respectively, which are calculated at pressure  $P$  and temperature  $T$  as

$$\gamma_L = \gamma_0 \frac{P}{P_0} \left( \frac{T_0}{T} \right)^{0.62}, \quad \gamma_D = \frac{\nu_0}{c} (2kT \ln 2 / m)^{1/2}, \quad (3)$$

where  $\gamma_0$  is the pressure broadened line-width at referenced pressure and temperature,  $P_0$  and  $T_0$ , respectively,  $\nu_0$  (cm<sup>-1</sup>) is the line center position, and  $m$  is the molecular weight [1].

The line strength  $S$  can be calculated from  $S_0$ , the line strength at referenced temperature  $T_0$ , as

$$S = S_0 \left( \frac{T_0}{T} \right)^{1.5} \exp \left[ \frac{E'' hc}{k} \left( \frac{1}{T_0} - \frac{1}{T} \right) \right], \quad (4)$$

where  $E''$  is the energy of the lower state,  $h$  is Planck's constant,  $c$  is the speed of light, and  $k$  is Boltzmann's constant [1].

The H<sub>2</sub>O absorption cross section  $\sigma_V(\nu)$  can be typically calculated based on the Voigt profile as

$$\sigma_V(\nu) = \sigma_V(\nu_0) \frac{y}{\pi} \int_{-\infty}^{+\infty} \frac{\exp(-t^2)}{y^2 + (x-t)^2} dt, \quad (5)$$

where  $\sigma_V(\nu_0)$  is the cross section at absorption line center, and

$$x = \left[ \frac{(\nu - \nu_0)}{\gamma_D} \right] \sqrt{(\ln 2)}, \quad y = \frac{\gamma_L}{\gamma_D} \sqrt{(\ln 2)}. \quad (6)$$

Using Whiting's expression, the H<sub>2</sub>O absorption cross section equation can be simply rewritten as [3]

$$\sigma_V(\nu) = \sigma_V(\nu_0) \left\{ (1-x) \exp(-0.693y^2) + \frac{x}{1+y^2} + 0.016(1-x)x \left[ \exp(-0.0841y^{2.25}) - \frac{1}{1+0.0210y^{2.25}} \right] \right\}, \quad (7)$$

$$\text{where } x = \frac{\gamma_L}{\gamma_D}, \quad y = \frac{|\nu - \nu_0|}{\gamma_V}, \quad (8)$$

$$\sigma_V(\nu_0) = \frac{S(T)}{2\gamma_V(1.065 + 0.447x + 0.058x^2)}, \quad (9)$$

and  $\gamma_V$  is the Voigt profile half-width at half-maximum as

$$\gamma_V = 0.5346\gamma_L + (0.2166\gamma_L^2 + \gamma_D^2)^{1/2}. \quad (10)$$

## 2.2 DIAL measurement errors

From Eq. 1, two types of DIAL measurement errors can be classified including signal detection error and cross section error. The H<sub>2</sub>O absorption cross section error is caused by the atmospheric effect as well as laser system characteristic. In the scope of this paper, the cross section error related to temperature sensitivity and laser wavelength uncertainty is evaluated to optimize selected operation wavelength.

The signal detection error is caused by the uncertainty of the detected signal, background signal, and dark current. The background signal  $B$  can be represented by

$$B = \frac{L}{h\nu} \cdot \frac{\rho}{\pi} \cdot \pi \left( \frac{\theta}{2} \right)^2 A\omega Q\eta \Delta t \exp(-2\tau), \quad (11)$$

where  $L$  is the solar irradiance value for a nominal two-way optical depth  $2\tau$  of 0.5,  $\omega$  is the optical filter width (FWHM),  $\rho$  is the surface reflectance, and  $\theta$  is the receiver field of view [1].

The dark current  $D$  is described as

$$D = \left( \frac{NEP}{\sqrt{2}} \eta \frac{\lambda}{hc} \right)^2 \Delta t, \quad (12)$$

where  $NEP$  is the noise equivalent power.

Consequently, the relative error in DIAL signal detection is calculated as follows

$$\frac{\Delta n}{n} = \frac{1}{2\Delta\sigma n(R_2 - R_1)} \left\{ \sum_{i=1}^2 \sum_{j=1}^2 \left[ \frac{(S_{ij} + B)F + D}{S_{ij}^2} \right] \right\}^{1/2} \quad (13)$$

where  $i=1,2$  is for the ranges  $R_1$  and  $R_2$ , respectively, and  $j=1,2$  is for the online and offline signals, respectively [1].

## III. OPTIMUM WAVELENGTH EVALUATION

In DIAL technique, a pair of neighbor wavelengths is selected to be on the peak of absorption line and off the absorbed region, respectively. The online wavelength is evaluated in near infrared range including 700nm-band, 800nm-band, and 900nm-band. The monthly mean profile at Tsukuba in Japan for both February and August are employed due to the H<sub>2</sub>O density differences as shown in Fig. 1. At the ground, the H<sub>2</sub>O density in August is over four times larger than one in February. The H<sub>2</sub>O DIAL parameters applied for this work are given in Table I.

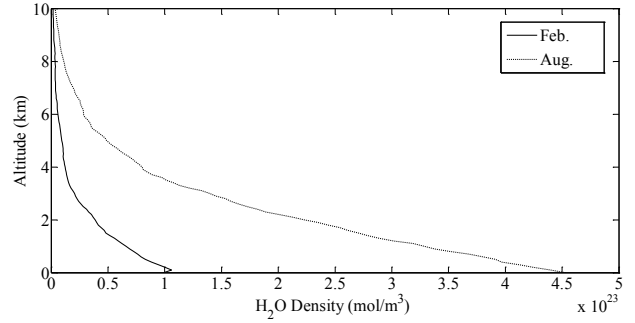


Fig. 1. H<sub>2</sub>O density in February (solid line) and August (dotted line) based on the monthly mean profile in Tsukuba, Japan.

In order to determine the optimum line strength for each wavelength-band, the maximum reached altitude of 700nm-band, 800nm-band, and 900nm-band lidar according to the relative error of less than 10% are calculated for day-time of February and August, respectively, as shown in Fig. 2. The 700nm-band and 800nm-band reach the highest altitude of around 3.6 km for January and 3.8 km for August, respectively, while 900nm-band reaches slightly lower altitude. The optimum line strength of each case is presented in Table II. As a result, the online-wavelengths are decided as 823.616 nm with the line strength of  $1.62e-23 \text{ cm}^{-1}/(\text{mol cm}^{-2})$  and 823.689 nm with the line strength of  $2.42e-24 \text{ cm}^{-1}/(\text{mol cm}^{-2})$  for February and August period, respectively, since they are near by each other and satisfy the optimum line strength condition. The H<sub>2</sub>O absorption line based on Voigt profile around the selected online wavelengths at the altitudes of 0 km and 10 km, respectively, are shown in Fig. 3.

Table I. The H<sub>2</sub>O DIAL parameters

Energy per pulse	1 $\mu$ J
Pulse width	1 $\mu$ s
Effective area of receiver	0.096 m <sup>2</sup>
Total optical efficiency of the receiver	29% (day-time) 49% (night-time)
Quantum efficiency: 700nm-band	50%
800nm-band	50%
900nm-band	30%
Noise equivalent power	2e-14 W Hz <sup>-1/2</sup>
Excess noise factor	2.5
Solar irradiance: 700nm-band	120 $\mu$ W cm <sup>-2</sup> nm <sup>-1</sup>
800nm-band	100 $\mu$ W cm <sup>-2</sup> nm <sup>-1</sup>
900nm-band	70 $\mu$ W cm <sup>-2</sup> nm <sup>-1</sup>
Filter bandwidth (day-time)	0.4 nm
Field of view	1.23 mrad
Accumulation time	1 hour
Repetition rate	10 kHz

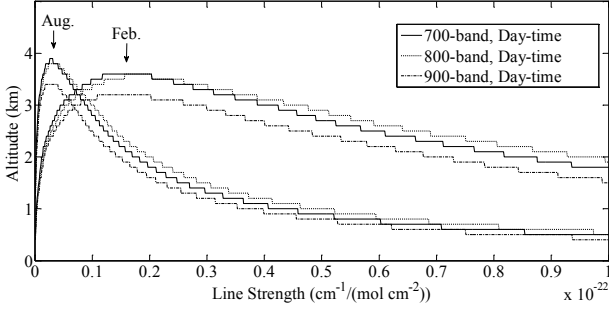


Fig. 2. Maximum reached altitude according to relative error of less than 10% for 700nm-band (solid line), 800nm-band (dotted line), and 900nm-band (dash-dot line) during day-time of February and August, respectively.

Table II. Optimum line strength

Wavelength	Line Strength (cm <sup>-1</sup> /(mol cm <sup>-2</sup> ))
700nm-band	[1.18e-23, 1.88e-23] (Feb.)
	[2.60e-24, 3.00e-24] (Aug.)
800nm-band	[1.57e-23, 2.03e-23] (Feb.)
	[2.40e-24, 3.90e-24] (Aug.)
900nm-band	[1.09e-23, 2.02e-23] (Feb.)
	[2.20e-24, 3.30e-24] (Aug.)

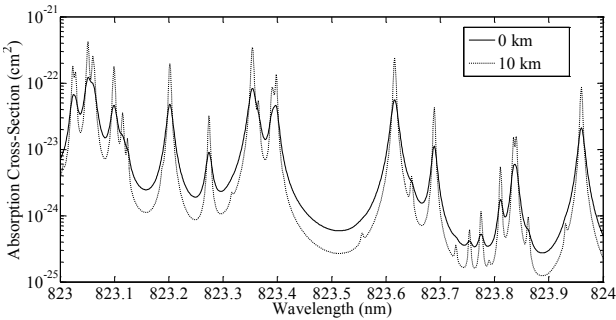


Fig. 3. Voigt profile of the water vapor absorption cross section around the selected operational lines at the altitudes of 0 km (solid line) and 10 km (dotted line), respectively.

The next stage is selecting the optimum offline-wavelength over the observed region. The offline-wavelength is evaluated in terms of temperature sensitive and laser wavelength uncertainty. The proposed parameters including temperature relative error and wavelength tuning error are used for these evaluations. By adjusting the temperature in a range of  $[T - 10K, T + 10K]$ , the temperature relative error is calculated as

Temperature Relative Error =

$$\frac{abs(\Delta\sigma_T - \Delta\sigma_{T-10K}) + abs(\Delta\sigma_T - \Delta\sigma_{T+10K})}{2\Delta\sigma_T} \quad (14)$$

where  $\Delta\sigma_{T-10K}$ ,  $\Delta\sigma_T$ ,  $\Delta\sigma_{T+10K}$  are the differential absorption cross section between the online and offline wavelengths at  $T - 10K$ ,  $T$ ,  $T + 10K$ , respectively. Figure 4 illustrates the results of temperature relative error over the varied offline-wavelength in February and August at the altitudes of 0 km and 10 km, respectively.

The wavelength uncertainty, represented by wavelength tuning error, is calculated as

Wavelength Tuning Error =

$$\frac{abs(\sigma_\lambda - \sigma_{\lambda-1pm}) + abs(\sigma_\lambda - \sigma_{\lambda+1pm})}{2\sigma_\lambda} \quad (15)$$

where  $\sigma_{\lambda-1pm}$ ,  $\sigma_\lambda$ , and  $\sigma_{\lambda+1pm}$  are the H<sub>2</sub>O absorption cross section at the wavelengths of  $\lambda - 1pm$ ,  $\lambda$ , and  $\lambda + 1pm$ , respectively. Figure 5 describes the wavelength tuning error around the selected operational lines at the altitudes of 0 km and 10 km, respectively.

Since all the relative error, temperature relative error, and wavelength tuning error play important roles in selecting offline-wavelength, the proposed root-mean-square error (RMSE) takes over as

$$RMSE = \sqrt{\frac{1}{3} (Temperature\ Relative\ Error^2 + Wavelength\ Tuning\ Error^2 + Relative\ Error^2)} \quad (16)$$

Consequently, the maximum reached altitude with the RMSE of less than 10% for the pair of online-wavelengths of 823.616 nm for February and 823.689 nm for August, respectively, and varied offline-wavelength in the range of 823.4 nm to 823.8 nm are plotted in Fig. 6. As a result, the offline-wavelength of 823.763 nm is selected due to its highest reached altitude of 4.9 km for night-time February, 4.3 km for day-time February, 4.8 km for night-time August, and 4.4 km for day-time August.

The selected operational wavelengths are compared with the referenced wavelengths utilized in Nehrir et al., including the online-wavelength of 828.187 nm and the offline-wavelength of 828.287 nm [4]. Similarly, Figure 7 illustrates the maximum reached altitude with the RMSE of less than 10% for the pair of referenced online-wavelength of 828.187 nm and the varied offline-wavelength in the range of 828 nm to 828.4 nm during day-time and night-time of February and August, respectively. As a result, the maximum altitude of a pair of the referenced wavelengths in February reaching 4.9

km for night-time and 4.3 km for day-time is the same as the one of selected wavelengths. However, the maximum altitude of a pair of the referenced wavelengths in August reaching 2.7 km for night-time and 2.6 km for day-time is significantly lower than the one of the selected wavelengths. It is evident that the referenced wavelengths is not appropriate for operating lidar system over Japan.

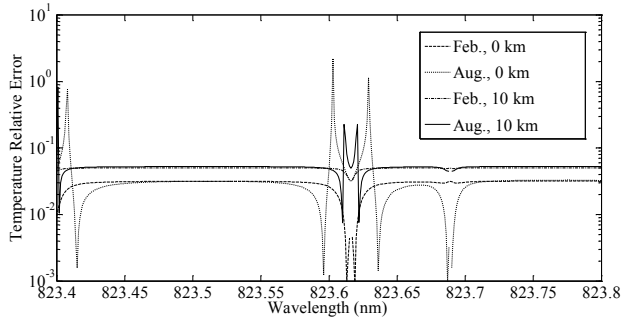


Fig. 4. Temperature relative error of the pair of the online-wavelength (823.616 nm for February and 823.689 nm for August) and varied offline-wavelength (from 823.4 nm to 823.8 nm) at the altitudes of 0 km and 10 km, respectively.

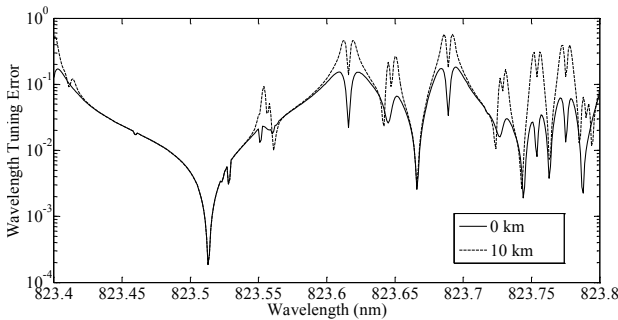


Fig. 5. Wavelength tuning error around the selected operational lines at the altitudes of 0 km (solid line) and 10 km (dotted line), respectively.

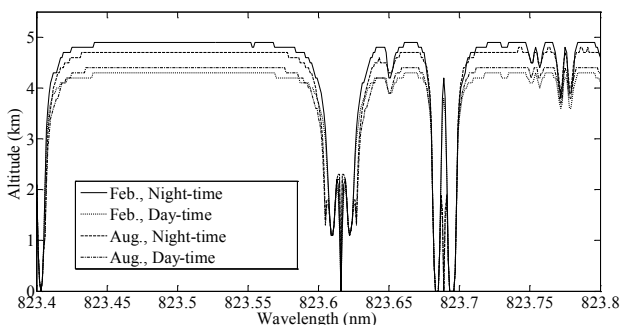


Fig. 6. Maximum reached altitude according to the RMSE of less than 10% for the pair of online-wavelength (823.616 nm for February and 823.689 nm for August) and varied offline-wavelength (from 823.4 nm to 823.8 nm) during day-time and night-time, respectively.

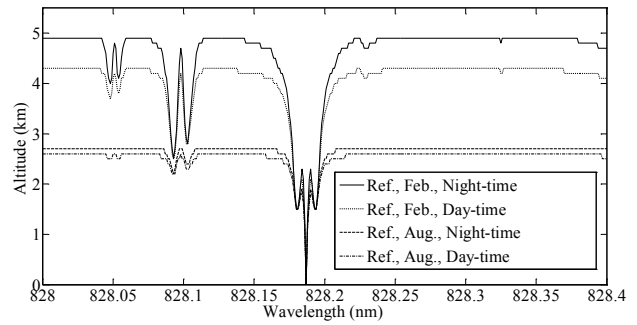


Fig. 7. Maximum reached altitude according to the RMSE of less than 10% for the pair of referenced online-wavelength (828.187 nm for both February and August) and varied offline-wavelength (from 828 nm to 828.4 nm) during day-time and night-time, respectively.

#### IV. CONCLUSIONS

In this paper, the process of advanced wavelength selection for diode laser based water vapor differential absorption lidar is described. The relative error, temperature relative error, and wavelength tuning error simultaneously distribute to the decision making of online and offline wavelength. Consequently, the online-wavelength of 823.616 nm for February and 823.689 nm for August and the offline-wavelength of 823.763 nm are selected. In the future work, these wavelengths will be utilized in our developing lidar system over Japan.

#### ACKNOWLEDGEMENT

The authors gratefully acknowledge the financial sponsor from the Tokyo Metropolitan Government in AHRF scholarship for Mr. Phong Pham Le Hoai.

#### REFERENCES

- [1] S. Ismail and E. V. Browell, "Airborne and space borne lidar measurements of water vapor profiles: a sensitivity analysis," *Appl. Opt.*, Vol. 28, No. 17, 3603-3615 (1989).
- [2] R. A. McClatchey *et al.*, "Optical Properties of the Atmosphere," Air Force Geophys. Lab., Hanscom AFB, AFCRL 72-0497 (1972).
- [3] M. Gharavi and S. G. Buckley, "Single Diode Laser Sensor for Wide-Range H<sub>2</sub>O Temperature Measurements," *Applied Spectroscopy*, Vol. 58, Issue 4, 468-473 (2004).
- [4] A. R. Nehrir *et al.*, "Micropulse water vapor differential absorption lidar: transmitter design and performance," *Optics Express*, Vol. 20, Issue 22, 25137-25151 (2012).